Finite-temperature phase structures of hard-core bosons in an optical lattice with an effective magnetic field

Yuki Nakano, Kenichi Kasamatsu, and Tetsuo Matsui
Department of Physics, Kinki University, Higashi-Osaka, Osaka 577-8502, Japan
(Dated: February 24, 2012)

We study finite-temperature phase structures of hard-core bosons in a two-dimensional optical lattice subject to an effective magnetic field by employing the gauged CP^1 model. Based on the extensive Monte Carlo simulations, we study their phase structures at finite temperatures for several values of the magnetic flux per plaquette of the lattice and mean particle density. Despite the presence of the particle number fluctuation, the thermodynamic properties are qualitatively similar to those of the frustrated XY model with only the phase as a dynamical variable. This suggests that cold atom simulators of the frustrated XY model are available irrespective of the particle filling at each site.

PACS numbers: 03.75.Hh 67.85.Hj 05.70.Fh 64.60.De

I. INTRODUCTION

Ultracold atoms in an optical lattice (OL) have been a particularly important field to study a wide range of fundamental problems in condensed matter physics [1]. When an OL is rotated, we can expect versatile cold-atom quantum simulators, which can demonstrate various effects caused by a magnetic field such as quantum Hall effects [2]. This is because the neutral atoms in a rotating reference frame experience a Coriolis force of the same form as the Lorentz force on charged particles in a magnetic field. Recently, two experiments were reported, making use of a rotating OL to study quantized vortices in gaseous Bose-Einstein condensates (BECs) [3, 4]. Moreover, "synthesis" of a gauge field was realized by using a spatially varying Raman coupling between internal atomic states to implement the required geometric phases [5–8], opening a door to more wide ranging studies associated with an artificial magnetic field that gives rise to an orbital motion of neutral atoms.

The Bose-Hubbard model under an effective magnetic field exhibits very interesting physics [9–23], far beyond the physics of the usual Bose-Hubbard model. These properties are inherited from the remarkable structure of the energy spectrum for noninteracting problems, i.e., a single particle moving on a tight-binding lattice in the presence of a uniform magnetic field. Here, the energy spectrum depends sensitively on the frustration parameter f, a magnetic flux per plaquette of the lattice, and exhibits a fractal structure known as the "Hofstadter butterfly" [24]. For a rational value $f = p/q$ (with the integers p and q), there are q bands, and each state is q-fold degenerate [25, 26]. A series of theoretical proposals indicates that it should be possible to implement strong gauge fields such as $f \sim 1$ on an OL [9–12]. In fact, it has been experimentally demonstrated recently [8]. In the strongly interacting regime, where both the particle number per site and the magnetic flux per plaquette are of order unity, it is theoretically predicted that there exist strongly correlated phases representative of the continuum quantum Hall states [11, 16, 18]. In the weakly-interacting condensed phase under the strong magnetic field, the frustrated Josephson junction arrays provide a close analog of that system, and implementations using cold atoms have been proposed [27, 28].

These studies focused mainly on the ground-state properties and the quantum phase transitions at *zero temperature*. However, they are mostly based on the exact diagonalization study and are restricted to small systems. In this paper, we study the *finite-temperature* phase diagram of hard-core bosons in a two-dimensional (2D) OL with an effective gauge field. Our study is relevant to atoms with low densities and very strong repulsive interactions, e.g., tuned by the Feshbach resonance [29]. In the hard-core limit, the Bose-Hubbard model can be mapped to the quantum spin model and described by the CP^1 (complex projective) operators, which are useful to construct the path-integral formulation [30]. In the high-temperature limit, the quantum Hamiltonian reduces to the classical *three-component* XY model [i.e., without nearest-neighbor s_z coupling as shown in Eq.(10) below] frustrated by the gauge field, which is referred to as the gauged CP^1 model below. This reduction provides a practical platform to explore the finite-temperature phase diagram of this system and to discuss the detailed critical properties of the phase transitions.

It is known that the 2D frustrated XY model (FXYM), which has only two components s_x and s_y, is closely related to our model and exhibits very rich properties of the phase transition [31–41]. For the fully frustrated XY model (FFXYM) with $f = 1/2$, there would be double phase transitions, one is associated with the Berezinskii-Kosterlitz-Thouless (BKT) transition due to the global U(1) symmetry and the other associated with Ising-model-like transition due to the Z_2 chiral symmetry of the ground state. A central issue in the studies of the FFXYM has been to clarify how these two distinct types of orderings take place [31]. One possibility is that, even at the temperature where the Z_2 chirality establishes a long-range order at $T < T_c$, the U(1) phase (XY-spin) may remain disordered due to thermally excited, unbound vortices. Then, the orderings of the two vari-

ables take place at two separate temperatures such that $T_c > T_{\rm BKT}$. The other possibility is that both orderings of the chirality and the phase take place at the same temperature, and the resulting single phase transition is neither of the conventional Ising type nor the BKT type but follows a new universality class. Many studies have discussed this phase transition, but yet do not provide conclusive results. The phase transitions for other values of f, e.g., $f = 1/3$, $2/5$, etc., were also discussed in Refs. [42–45].

Our study is an extension of these studies by incorporating the particle number fluctuation (z-component of the spin) at each site. It is nontrivial how the additional degree of freedom has an influence on the above thermodynamic properties. To the best of our knowledge, the statistical properties of this model have not been considered so far. We confine ourselves to the values of the frustration parameter $f = 0$, $1/2$, and $2/5$ to settle the discussion, and make a comparison with the results obtained by the usual XY model. Although our concerning model is a classical one (obtained by neglecting the quantum fluctuations relevant at low temperatures), this should properly describe the thermodynamic properties of the hard-core bosons in an optical lattice at sufficiently high temperatures [46].

In Sec.II, we describe how to obtain our gauged CP^1 model, starting from the Bose-Hubbard Hamiltonian with the gauge field. The ground-state properties of the gauged CP^1 model are discussed in Sec. III. In Sec. IV, based on the Monte-Carlo simulations, we study the finite-temperature phase structures of the gauged CP^1 model for the averaged site occupation of hard-core bosons being half-filled and non-half-filled. Section V is devoted to conclusions and discussion.

II. MODEL

A. Hamiltonian for hard-core bosons in an effective magnetic field

We consider a system of N-bosons put on the sites of a 2D square lattice with the size $L \times L$. The 2D Bose-Hubbard model subject to a uniform Abelian gauge potential is described by the Hamiltonian

$$\hat{H} = -\frac{t}{2}\sum_{\langle i,j\rangle}\left[\hat{a}_i^\dagger \hat{a}_j e^{iA_{ij}} + \text{h.c.}\right] + \frac{U}{2}\sum_i \hat{\rho}_i(\hat{\rho}_i - 1) - \mu\sum_i \hat{\rho}_i. \quad (1)$$

Here, the operator $\hat{a}_i^{(\dagger)}$ destroys (creates) a boson on the lattice site $i = (i_x, i_y)$. $\langle i,j\rangle$ implies a pair of nearest-neighbor sites. t, μ, and $U(\geq 0)$ describe the nearest-neighbor tunneling energy, the chemical potential, and the onsite repulsion, respectively. $\hat{\rho}_i = \hat{a}_i^\dagger \hat{a}_i$ is the number operator at i and the Hamiltonian conserves the total number of bosons, $\hat{N} = \sum_i \hat{\rho}_i$. Throughout this work, we consider the system without additional trap potentials such as a harmonic one. Nevertheless, the results of this study can be applied within the local density approximation to realistic experimental systems which have an additional trapping potential.

The field A_{ij} describes the imposed gauge potential, defined by $A_{ij} = \int_{\mathbf{r}_j}^{\mathbf{r}_i} \mathbf{A}\cdot d\mathbf{r}$. All of the physics of the system governed by the Hamiltonian (1) is gauge-invariant. Hence, its properties depend only on the magnetic fluxes of magnitude B through plaquettes

$$\Phi = \int_{\rm plaq} d\mathbf{S}\cdot\mathbf{B} = \sum_{i,j\in\alpha} A_{ij} = Bd^2 = 2\pi f, \quad (2)$$

where α labels the plaquette, and the sum represents the directed sum of the gauge fields around that plaquette (the discrete version of the line integral). d is a typical lattice spacing and the last equality relates B and f. In the following, we use the vector potential in the symmetric gauge and its form can be written as

$$\mathbf{A} = (A_x, A_y, A_z) = \left(-\frac{B}{2}y, \frac{B}{2}x, 0\right). \quad (3)$$

This corresponds to a uniform magnetic field $\mathbf{B} = (0, 0, B)$ in the direction perpendicular to the lattice plane. The discrete vector potential is then written as

$$A_{ij} = \begin{cases} -\pi f i_y & \text{for } i = (i_x, i_y),\ j = (i_x+1, i_y) \\ \pi f i_x & \text{for } i = (i_x, i_y),\ j = (i_x, i_y+1). \end{cases} \quad (4)$$

In the following, we take a hard-core limit ($U \to \infty$), where the allowed physical states at i are eigenstates of $\hat{\rho}_i$ with eigenvalue 0 or 1 and their superpositions. States with higher particle number at the same site such as double occupancy are excluded. We introduce a destruction operator of the hard-core boson as $\hat{\phi}_i$, which satisfies the following mixed canonical-(anti)commutation relations

$$\left[\hat{\phi}_i, \hat{\phi}_j\right] = 0, \quad \left[\hat{\phi}_i, \hat{\phi}_j^\dagger\right] = 0 \ \text{ for } \ i \neq j, \quad (5)$$

and on the same site,

$$\left\{\hat{\phi}_i, \hat{\phi}_i\right\} = 0, \quad \left\{\hat{\phi}_i, \hat{\phi}_i^\dagger\right\} = 1. \quad (6)$$

Thus, the number operator is rewritten as $\hat{\rho}_i = \hat{\phi}_i^\dagger\hat{\phi}_i$ and its eigenvalue ρ_i is assured to be 0 or 1. Then, the Hamiltonian $\hat{H}$ is written as

$$\hat{H}_{\rm hc} = -\frac{t}{2}\sum_{\langle i,j\rangle}\left(\hat{\phi}_i^\dagger\hat{\phi}_j e^{iA_{ij}} + \text{H.c.}\right) - \mu\sum_i \hat{\phi}_i^\dagger\hat{\phi}_i, \quad (7)$$

where μ determines the mean density ρ of hard-core bosons per site,

$$\rho \equiv \langle\bar{\rho}\rangle, \qquad \bar{\rho} \equiv \frac{1}{L^2}\sum_i \hat{\phi}_i^\dagger\hat{\phi}_i, \quad (8)$$

within the range $0 \leq \rho \leq 1$.

In the hard-core limit, the Bose-Hubbard model becomes equivalent to a spin-1/2 quantum magnet, because the following relations exist between $\hat{\phi}_i$ and the $s = 1/2$ SU(2) spin operator $\hat{s}_i^{x,y,z}$ [30],

$$\hat{s}_i^z = \hat{\phi}_i^\dagger \hat{\phi}_i - \frac{1}{2}, \quad \hat{s}_i^+ \equiv \hat{s}_i^x + i\hat{s}_i^y = \hat{\phi}_i^\dagger, \quad \hat{s}_i^- = \hat{\phi}_i,$$
$$(\hat{s}_i^x)^2 + (\hat{s}_i^y)^2 + (\hat{s}_i^z)^2 = \frac{3}{4}. \tag{9}$$

The Hamiltonian (7) then becomes

$$\hat{H}_{\rm hc} = -\frac{t}{2} \sum_{\langle i,j \rangle} \left(\hat{s}_i^+ \hat{s}_j^- e^{iA_{ij}} + \hat{s}_j^+ \hat{s}_i^- e^{-iA_{ij}} \right) - \mu \sum_i \hat{s}_i^z. \tag{10}$$

Here, the conservation of total particle number is interpreted as the constant magnetization $\hat{S}^z = \sum_i \hat{s}_i^z$. Under Eq.(9), the eigenstates have the correspondence $|\uparrow_i\rangle = |\rho_i = 1\rangle$ and $|\downarrow_i\rangle = |\rho_i = 0\rangle$. This Hamiltonian describes a quantum spin-1/2 magnet, experiencing XY nearest neighbor spin exchange interactions. These exchange interactions are frustrated due to the gauge field A_{ij}.

B. CP^1 variable and path-integral representation

To study the thermodynamic properties of this system, we evaluate the partition function Z of the grand canonical ensemble,

$$Z = {\rm Tr} e^{-\beta \hat{H}_{\rm hc}}, \quad \beta = \frac{1}{k_B T}. \tag{11}$$

We express Z by a path integral which is useful for numerical calculations. For this purpose, it is convenient to introduce a CP^1 variable $w_i = (w_{1i}, w_{2i}) \in C$ which satisfies the CP^1 constraint,

$$|w_{1i}|^2 + |w_{2i}|^2 = 1. \tag{12}$$

An associated pseudocoherent state $|w_i\rangle$ is defined by

$$|w_i\rangle \equiv w_{1i}|\uparrow_i\rangle + w_{2i}|\downarrow_i\rangle, \tag{13}$$

where $|w_i\rangle$ is normalized as $\langle w_i|w_i\rangle = 1$ due to Eq. (12), and we have generally $\langle w_i|w_i'\rangle = w_{i1}^* w_{i1}' + w_{i2}^* w_{i2}' = w_i^* w_i'$. Let us define the integration measure

$$\int [d^2 w_i] \equiv 2 \int_C d^2 w_{1i} \int_C d^2 w_{2i} \delta \left(\langle w_i|w_i\rangle - 1 \right) \tag{14}$$

which satisfies

$$\int [d^2 w_i] 1 = 2, \quad \int [d^2 w_i] w_{ia}^* w_{ib} = 2 \times \frac{1}{2} \delta_{ab} = \delta_{ab}. \tag{15}$$

Then the completeness is expressed as

$$\int [d^2 w_i] |w_i\rangle\langle w_i| = |\uparrow_i\rangle\langle\uparrow_i| + |\downarrow_i\rangle\langle\downarrow_i| = 1. \tag{16}$$

The Hamiltonian can be represented by the CP^1 operators $\hat{w}_{1i}$ and $\hat{w}_{2i}$ which satisfy the bosonic commutation relation

$$[\hat{w}_{ai}, \hat{w}_{bj}] = 0, \quad [\hat{w}_{ai}, \hat{w}_{bj}^\dagger] = \delta_{ab}\delta_{ij}, \quad a, b = 1, 2, \tag{17}$$

and their physical states are restricted as $\sum_a \hat{w}_{ai}^\dagger \hat{w}_{ai} |{\rm phys}\rangle = |{\rm phys}\rangle$. Here, the correspondence to the spin operator is given as

$$|\uparrow_i\rangle = \hat{w}_{1i}^\dagger |{\rm vac}\rangle, \quad |\downarrow_i\rangle = \hat{w}_{2i}^\dagger |{\rm vac}\rangle, \tag{18}$$

and

$$\hat{s}_i^{x,y,z} = \frac{1}{2} (\hat{w}_{1i}^\dagger, \hat{w}_{2i}^\dagger) \sigma^{x,y,z} (\hat{w}_{1i}, \hat{w}_{2i})^t,$$
$$\hat{s}_i^z = \hat{w}_{1i}^\dagger \hat{w}_{1i} - \frac{1}{2}, \quad \hat{s}_i^+ = \hat{w}_{1i}^\dagger \hat{w}_{2i}, \quad \hat{s}_i^- = \hat{w}_{2i}^\dagger \hat{w}_{1i}, \tag{19}$$

where $\sigma^{x,y,z}$ are Pauli matrices. Equations (19) and (9) imply the relation $\hat{\phi}_i = \hat{w}_{2i}^\dagger \hat{w}_{1i}$, etc. We also note the following relation :

$$\langle w_i'|\hat{w}_{ia}^\dagger \hat{w}_{ib}|w_i\rangle = (w_{ia}')^* w_{ib}. \tag{20}$$

Using these relations and following the standard procedure, we can write the partition function Z in the path-integral form with the imaginary time $\tau \in [0, \beta]$ as

$$Z = \prod_{i,\tau} \int [d^2 w_i(\tau)] e^{\int_0^\beta d\tau A(\tau)}, \tag{21}$$

where

$$A(\tau) = -\sum_{i,a} w_{ai}^*(\tau) \dot{w}_{ai}(\tau)$$
$$+ \frac{t}{2} \sum_{\langle i,j \rangle} \left(w_{1i}^*(\tau) w_{2i}(\tau) w_{2j}^*(\tau) w_{1j}(\tau) e^{iA_{ij}} + {\rm c.c.} \right)$$
$$+ \mu \sum_i w_{1i}^*(\tau) w_{1i}(\tau). \tag{22}$$

Here, the CP^1 operators have been replaced to the complex numbers by employing the path-integral formulation.

To proceed further, we make one simplification by considering the finite-T region, such that the τ-dependence of $w_{ai}(\tau)$ in the path integral can be ignored, keeping only the zero modes as $w_{ai}(\tau) \to w_{ai}$ [46]. This corresponds to neglecting the quantum fluctuations. As a result, the problem is reduced to the classical one. Under the relations (9) and (19), one can finally obtain

$$Z = \prod_i \int [d^2 w_i] e^{-\beta H_{\rm CP^1}(w)}, \tag{23}$$

where $H_{\rm CP^1}(w)$ is the classical version of Eq. (7) expressed in terms of w_i:

$$H_{\rm CP^1}(w) = -\frac{t}{2} \sum_{\langle i,j \rangle} \left(\phi_i^* \phi_j e^{iA_{ij}} + {\rm c.c.} \right) - \mu \sum_i w_{1i}^* w_{1i},$$
$$\phi_i \equiv w_{2i}^* w_{1i}. \tag{24}$$

This allows us to study the finite-T phase structure, which summarizes the essential properties of the system. Besides, the finite-T phase diagram gives a very useful insight into the phase structure at $T = 0$; if some ordered states are found at finite T, we can naturally expect that they persist down to $T = 0$. Equation (24) is referred to as the "gauged CP^1 model" in the following [47]. We can evaluate the partition function of Eq. (23) to understand the thermodynamic properties of the system, using the standard Monte Carlo simulations. From the symmetry properties summarized in Appendix A, we can confine ourselves to $0 \le f \le 1/2$ and $1/2 \le \rho \le 1$ in the following argument.

We note that Eq.(24) is viewed as a gauged model of three-component normalized classical spin $\vec{s}_i$ [O(3) spin] [48] as

$$\begin{aligned} \vec{s}_i &\equiv w_i^\dagger \vec{\sigma} w_i, \quad \vec{s}_i \cdot \vec{s}_i = 1, \\ H_{\mathrm{CP}^1}(w) &= -\frac{t}{8} \sum_{\langle i,j \rangle} \left(s_i^+ s_j^- e^{iA_{ij}} + \text{c.c.} \right) - \frac{\mu}{2} \sum_i s_i^z, \\ [d^2 w_i] &= \frac{1}{\pi} d^3 \vec{s}_i \; \delta(\vec{s}_i \cdot \vec{s}_i - 1). \end{aligned} \tag{25}$$

C. Relation between the CP^1 model and the other models

Our model is an extended version of the FXYM,

$$H_{\mathrm{XY}} = -J \sum_{\langle i,j \rangle} \cos(\theta_i - \theta_j + A_{ij}). \tag{26}$$

To see this, we rewrite the CP^1 variables as

$$w_i = \begin{pmatrix} w_{1i} \\ w_{2i} \end{pmatrix} = \begin{pmatrix} \cos(\psi_i/2)\, e^{i\lambda_{1i}} \\ \sin(\psi_i/2)\, e^{i\lambda_{2i}} \end{pmatrix}. \tag{27}$$

Here, the angle variables have the ranges $0 \le \psi_i \le \pi$, $0 \le \lambda_{1i,2i} \le 2\pi$. The Hamiltonian Eq. (24) can be written as

$$H_{\mathrm{CP}^1} = -\frac{t}{4} \sum_{\langle i,j \rangle} \sin\psi_i \sin\psi_j \cos(\theta_i - \theta_j + A_{ij}) - \frac{\mu}{2} \sum_i \cos\psi_i, \tag{28}$$

with $\theta_i = \lambda_{2i} - \lambda_{1i}$ and the integration measure $[d^2\omega_i] = (4\pi^2)^{-1} \sin\psi_i d\psi_i d\lambda_{1i} d\lambda_{2i}$. The O(3) spin of Eq. (25) is expressed as

$$s_i^x = \sin\psi_i \cos\theta_i, \; s_i^y = \sin\psi_i \sin\theta_i, \; s_i^z = \cos\psi_i. \tag{29}$$

If we restrict the configuration space with fixed $\psi_i = \pi/2$, the ground state has (uniform) density $\rho = 1/2$, so that $s_i^z = 0$ and all the spins lie in the xy-plane. Then, the Hamiltonian reduces to the FXYM [Eq. (26)]. Here, "frustration" refers to the fact that, with $f \neq 0$ for any plaquette, the angles θ_i around this plaquette cannot be chosen to maximally satisfy the XY exchange couplings. The CP^1 model has a site-dependent factor $\sin\psi_i \sin\psi_j$ associated with the variation of the particle number at each site. Hence, the CP^1 model includes the particle number fluctuation and goes beyond the XY model based on the phase fluctuation only.

If we take into account the nearest-neighbor repulsive interaction in the Bose-Hubbard model, the hard-core constraint yields the gauged spin-half quantum XXZ model [49]

$$\hat{H}_{\mathrm{XXZ}} = -\frac{t}{2} \sum_{\langle i,j \rangle} \left(\hat{s}_i^+ \hat{s}_j^- e^{iA_{ij}} + \text{c.c.} \right) + V \sum_{\langle i,j \rangle} \hat{s}_i^z \hat{s}_j^z - \mu \sum_i \hat{s}_i^z. \tag{30}$$

Our model corresponds to the classical version of the gauged XXZ model with $V = 0$, called the XX0 (three-component XY) model [50]. The XX0 model is clearly distinct from the XY (two-component XY) model, as the spins fluctuate also out of the xy plane. In other words, even if the XX0 model and the XY model share the same form of the Hamiltonian, the associated phase space is different.

In addition, we note that there is a similar model in which the spins are random in not only their direction but also their magnitudes, known as the "fuzzy" spin XY model, [51]

$$H_{\mathrm{FXY}} = -J \sum_{\langle i,j \rangle} x_i x_j \cos(\theta_i - \theta_j). \tag{31}$$

While the magnitudes x_i of spins in the fuzzy XY model can have any values randomly and continuously site by site, the magnitude of O(3) spin $\vec{s}_i$ at each site in the CP^1 model is fixed unity, as shown in Eq. (25).

In the following, we compare the thermodynamic properties of our gauged CP^1 model Eq. (28) and the FXYM Eq. (26). The latter has been extensively studied for decades [31–41]. To this end, we have to put the two models in the same energy measure by establishing a relation between J and t. By noting the argument given below Eq. (29), let us try to replace the density at site i in Eq. (28) to the average value ρ, i.e., $\sin\psi_i \sin\psi_j \to \sin^2\psi$ with

$$\sin^2\psi = 4\cos^2\frac{\psi}{2}\left(1 - \cos^2\frac{\psi}{2}\right) = 4\rho(1-\rho), \tag{32}$$

where we have used $\rho \simeq \langle \phi^* \phi \rangle = \langle w_1^* w_1 \rangle = \cos^2(\psi/2)$. This correspondence implies the relation $J = t\rho(1-\rho)$. We use this relation when the energies in the two models (26) and (28) are compared. Note that this relation reflects the particle-hole symmetry and is *different from* the naive replacement $J = t\rho$.

III. GROUND STATE

We discuss here the ground-state properties of the CP^1 model. It is expected that the ground state exhibits similar behaviors to the FXYM, where the magnetic flux forms the typical pattern with the $q \times q$ unit cell structures for $f = p/q$; the checkerboard pattern emerges for $f = 1/2$ and the staircase pattern for $1/3 \leq f \leq 1/2$ [52–54]. Since the CP^1 model has an additional degree of freedom associated with the density fluctuation, it is expected that there are some differences from the results of the FXYM.

We calculate numerically the ground state of the gauged CP^1 model for fixed ρ by the simulated annealing method. Two examples for $\rho = 0.5$ and 0.95 are shown in Fig. 1, where the former corresponds to $\mu = 0$ (see Appendix A) while the latter is obtained by adjusting a proper value of μ for a given f. Figures 1 (a) and 1 (b) represent the ground-state energy $E_{\min}$ as a function of f. We also plot the energy for the FXYM for comparison. The shape of the energy curve is non-monotonic behavior with respect to f, following the bottom of the energy spectrum of the Hofstadter butterfly [54].

For $\rho = 0.5$ the ground-state energy coincides completely with that of the XY model. This is clear because ψ_i is freezed to $\pi/2$ at $\rho = 0.5$ and the particle-number does not fluctuate. Because $s_i^z = 0$ there, the ground-state properties are not affected at all even for $f \neq 0$. As ρ deviates from 0.5, the ground-state energy of the CP^1 model becomes slightly lower than that of the XY model, except for $f = 0.5$, as shown in Fig. 1(b).

Figures 1(c) and 1(d) show the distribution of the mean density $\rho_{\bar{i}}$ and the vorticity $m_{\bar{i}}$ at the site of the dual lattice $\bar{i}$, defined by

$$\rho_{\bar{i}} = \frac{1}{4}\sum_{i\in\alpha}\rho_i \quad m_{\bar{i}} = \frac{1}{2\pi}\sum_{i,j\in\alpha}(\theta_i - \theta_j + A_{ij}), \qquad (33)$$

where $|\theta_i - \theta_j + A_{ij}| \leq \pi$. The pattern of m_α constitutes the structure of a $q \times q$ unit cell, being similar to that of the FXYM. As discussed above, the ground-state particle density for $\rho = 0.5$ becomes uniform for any values of f. For $\rho \neq 0.5$, however, the mean density is also modulated spatially in accordance with the distribution of vorticity except for $f = 1/2$. This is the reason why the ground-state energy of the CP^1 model is lower than the XY model.

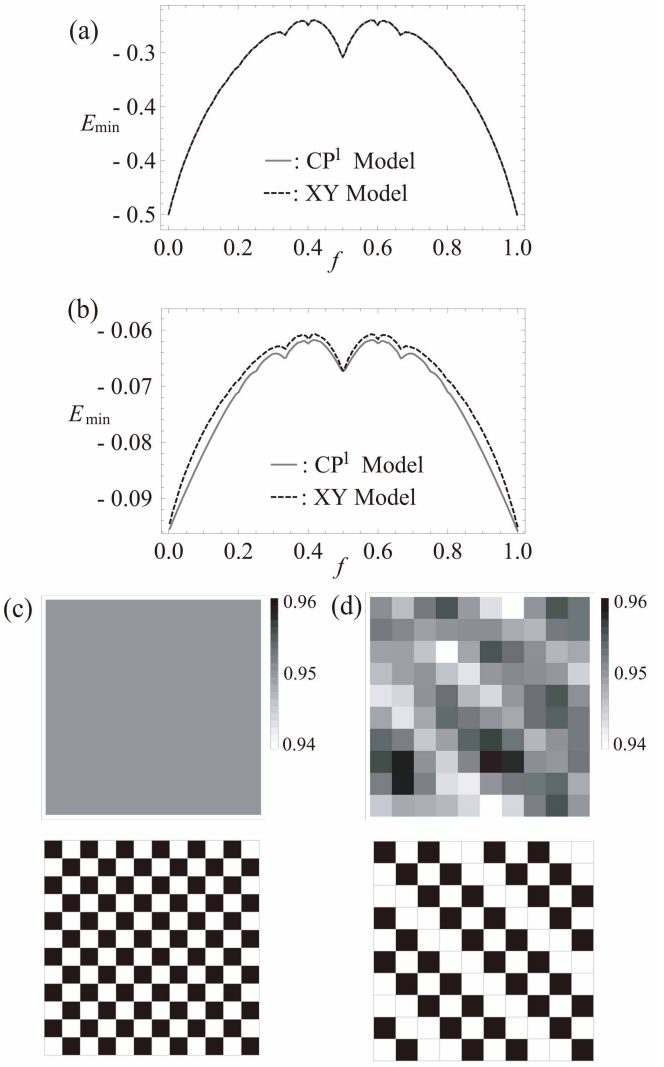

FIG. 1: The ground-state energy per site of the CP^1 model Eq. (28) as a function of the magnetic flux f for the averaged density (a) $\rho = 0.5$ and (b) 0.95, obtained through the simulated annealing. The solid curve denotes the energy of the CP^1 model without the chemical-potential term, while the dashed curve denotes that of the XY model with setting $J = t\rho(1-\rho)$ for comparison. The two curves overlap completely in (a); see the text for the reason. (c) and (d) show the distribution over the lattice ($L = 12$ and 10 for $f = 1/2$ and 2/5, respectively) of the mean density $\langle\rho_{\bar{i}}\rangle$ (the upper panels) and the vorticity $m_{\bar{i}}$ (the lower panels) at each plaquette $\bar{i}$ (the site of the dual lattice) for $\rho = 0.95$; (c) $f = 1/2$ and (d) $f = 2/5$.

IV. PHASE STRUCTURES AT FINITE T

We next turn to the discussion on the finite-temperature phase structures of the gauged CP^1 model and compare the result with the FXYM of Eq. (26). As described in Sec. I, the FFXYM with $f = 1/2$ may give rise to a nontrivial double phase transition [31–41] associated with the Ising transition apart from the BKT transition which is normally present at $f = 0$. In addition, there have been some discussions on the phase transitions for $f = 2/5$ and $f = 1/3$ [42–45]; their nature is dominated by the properties of the domain walls, following the Ising-like transition for $f = 1/3$ and the first-order transition for $f = 2/5$. Our primary interest is to see how an additional degree of freedom, associated with the particle number fluctuation at each site, modifies these properties. We made multicanonical Monte

Carlo simulations [55] to calculate statistical averages of some quantities described below.

We study the thermodynamic properties by calculating the specific heat defined by

$$C = \frac{1}{L^2}\left(\langle H_{\mathrm{CP}^1}^2\rangle - \langle H_{\mathrm{CP}^1}\rangle^2\right). \tag{34}$$

This value can be useful to locate the first- and second-order phase transition. In addition, to study the BKT transition, we calculate the in-plane susceptibility defined as $\chi = \partial\langle\bar{\phi}\rangle/\partial(\beta h)|_{h\to 0}$ with the site-average of the hard-core boson field $\bar{\phi} = \sum_i \phi_i/V$, explicitly written as

$$\chi = \frac{1}{L^2}\left\langle \sum_{i,j} \phi_i^* \phi_j \right\rangle - \frac{1}{L^2}\left\langle \sum_i \phi_i^* \right\rangle \left\langle \sum_i \phi_i \right\rangle. \tag{35}$$

Here, an auxiliary term $-h\sum_i \phi_i$ was introduced in Eq. (24) to derive Eq. (35). The second term of the right-hand side of Eq. (35) vanishes because of the global U(1) symmetry. This value grows as $\chi \propto L^{2-\eta}$ with the system size L when the correlation function obeys the power-law behavior $\langle\phi_i^*\phi_j\rangle \propto r^{-\eta}$ (with $\eta \le 2$) due to the presence of the quasi-long range order. On the other hand, it remains finite for $L \to \infty$ when the correlation decays exponentially as $\langle\phi_i^*\phi_j\rangle \propto e^{-mr}$. The value η is an exponent for the in-plane correlations below the BKT transition temperature T_{BKT}, being dependent on the temperature. We can calculate the exponent, as a function of temperature, by fitting the susceptibility for several system sizes L to the above expression for each temperature. For the conventional XY model the critical temperature T_{BKT} can be estimated when χ grows as $L^{7/4}$, i.e., $\eta = 1/4$

Furthermore, we study the helicity modulus which is directly connected to the superfluid density. The helicity modulus Υ is a measure of the resistance to an infinitesimal spin twist $\Delta\theta$ across the system along one coordinate. More precisely, it is defined through the change of the total free energy F with respect to an infinitesimal twist on the spin configuration along, say, the x-axis $\theta_i - \theta_{i'} \to \theta_i - \theta_{i'} + \delta\theta$, where i' is the nearest-neighbor site of the i-site along the x-direction and $\delta\theta = \Delta\theta/L$. One readily finds

$$\Delta F = \Upsilon(\delta\theta)^2 + \mathcal{O}((\delta\theta)^4), \tag{36}$$

and Υ can be given as

$$\Upsilon = -\frac{1}{L^2}\left(\langle H_x\rangle + \beta\langle I_x^2\rangle\right), \tag{37}$$

where H_x is the x-bond part of the Hamiltonian at $\Delta\theta = 0$ and I_x is the total current in the x-direction. For the CP^1 model, they are written as

$$H_x = -\frac{t}{4}\sum_{\langle i,j\rangle_x} \sin\psi_i \sin\psi_j \cos(\theta_i - \theta_j + A_{ij}),$$
$$I_x = -\frac{t}{4}\sum_{\langle i,j\rangle_x} \sin\psi_i \sin\psi_j \sin(\theta_i - \theta_j + A_{ij}). \tag{38}$$

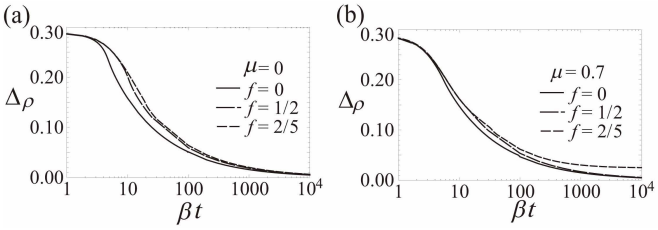

FIG. 2: The mean density ρ and the particle number fluctuation Δ_ρ as a function of $\beta\mu$ at the high-temperature or zero-hopping limit $\beta t \to 0$; the behavior is thus independent of f.

.

According to the renormalization-group theory, the helicity modulus for the conventional XY model in an infinite system jumps from zero to the finite value $(2/\pi)k_{\mathrm{B}}T_{\mathrm{BKT}}$ at the critical temperature $T = T_{\mathrm{BKT}}$ [56]. Therefore, a rough estimate of the critical temperature at a finite system could be obtained simply by locating the intersection of Υ as a function of T and the straight line $\Upsilon = 2k_{\mathrm{B}}T/\pi$.

In the FFXYM, the jump size has been suggested to be lager than the universal value [31–34, 41]. As a more accurate method to estimate both T_{BKT} and the jump size in the helicity modulus, an useful finite-size-scaling expression at $T = T_{\mathrm{BKT}}$ is known as [57]

$$\Upsilon(L, T = T_{\mathrm{BKT}}) = \frac{2}{\pi}k_{\mathrm{B}}T_{\mathrm{BKT}}^*\left(1 + \frac{1}{2}\frac{1}{\ln L + c}\right) \tag{39}$$

with T_{BKT}^* and c being fitting parameters. T_{BKT}^* is related to the jump size, being equal to T_{BKT} in the case of the usual XY model. By making a fit of the numerical data to Eq. (39) at various temperatures, one can estimate the transition temperature T_{BKT} as well as the critical exponent from the jump size as $\eta = T_{\mathrm{BKT}}/4T_{\mathrm{BKT}}^*$ [41, 58].

A. Density fluctuation

Before discussing the detailed thermodynamic properties, let us see the magnitude of the spatial fluctuation of the particle density, which is the important difference between the gauged CP^1 model and the FXYM. The particle density fluctuation is defined as

$$\Delta_\rho = \sqrt{\left\langle \frac{1}{L^2}\sum_i (\rho_i - \bar{\rho})^2 \right\rangle}, \tag{40}$$

which is zero for the XY model. In the high-temperature limit $\beta t \to 0$, one can calculate exactly the partition function $Z = [(e^{\beta\mu} - 1)/\beta\mu]^V$, and thus

$$\rho = \frac{1 + (-1 + \beta\mu)e^{\beta\mu}}{\beta\mu(-1 + e^{\beta\mu})}, \tag{41}$$

$$\Delta_\rho = \frac{-2 + (2 - 2\beta\mu + \beta^2\mu^2)e^{\beta\mu}}{\beta^2\mu^2(-1 + e^{\beta\mu})}, \tag{42}$$

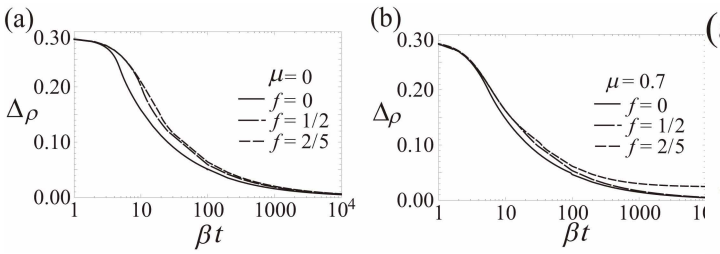

FIG. 3: The particle number fluctuation Δ_ρ as a function of βt for (a) $\mu = 0$ and (b) $\mu = 0.7$. The solid, dashed, and dotted curves correspond to $f = 0$, $1/2$, and $2/5$, respectively.

.

which are shown in Fig. 2. As one can see below [Fig. 9(a)], the mean density ρ is weakly dependent on βt for $\beta\mu \neq 0$. The density fluctuation Δ_ρ has a maximum at $\beta\mu = 0$, corresponding to half-filling $\rho = 1/2$, and decreases for $\beta\mu \to \pm\infty$. Since this Δ_ρ gives an upper limit of the expected particle number fluctuation, one can see that influence of the particle number fluctuation is less than 20% in a temperature range of our interest.

As seen in the ground state (Sec. III), the density becomes uniform for $\mu = 0$. Thus, Δ_ρ should go to zero as $\beta t \to \infty$ for $\mu = 0$. On the other hands, for $\mu \neq 0$, it must remains finite because the ground state possesses spatial density modulation. Figure 3 shows the βt-dependance of Δ_ρ for $\mu = 0$ and 0.7 for several values of f. For $\mu = 0$, Δ_ρ approaches to zero as $\beta t \to 0$ for any values of f. For $\mu = 0.7$, on the other hand, Δ_ρ approaches to zero as $\beta t \to 0$ only for $f = 1/2$, but remains finite for the other values of f. This behavior is consistent with the ground-state property shown in Fig. 1.

B. The case of half-filling ($\mu = 0$)

Here, we consider the case of half-filling $\rho = 0.5$ by setting $\mu = 0$. Then, the density distribution is completely uniform in the ground state, as seen in the complete overlap of the ground-state energy in Fig. 1(a), and thus the CP^1 model reproduces the ground state of the XY model. However, one has to take into account the density fluctuation at finite temperatures. This additional degree of freedom makes the finite-temperature phase diagram and the nature of the phase transition nontrivial. Here we focus on the case $f = 0$, $1/2$ and $2/5$, each of which has been known to give rise to quite different phase transitions in the FXYM.

1. *f=0*

First, we consider the situation of a zero magnetic field $f = 0$, which is useful to confirm the accuracy of our numerical computation. Then, the model is equivalent to the XX0 (three-component XY) model studied in Ref.

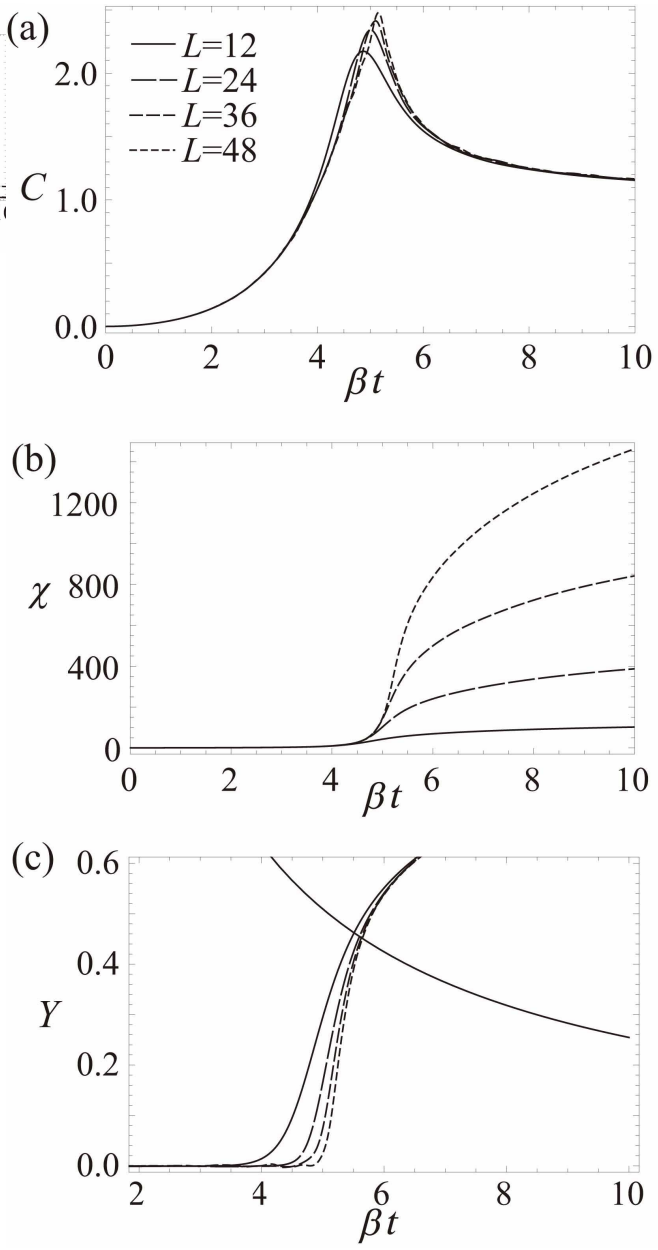

FIG. 4: Several thermodynamic quantities for f=0: (a) The specific heat C, (b) the in-plane susceptibility χ, and (c) the helicity modulus Υ for the CP^1 model with $\mu = 0$ and $f = 0$ as a function of βt. The system size for each curve is $L = 12$, 24, 36, 48. An additional curve $\Upsilon = 8/\pi\beta t$ in (c) indicates the universal jump of a BKT transition.

.

[50]. The phase transition of this model has been found to be consistent with the BKT theory. The specific heat C has very small finite-size effects. The in-plane susceptibility χ is a strongly increasing function of the system size L for low temperatures, while all the data fall on the same curve for high temperatures. These facts indicate the absence of second-order transition and the possibility of the BKT type transition involving the power-law decay

of the correlation function. The transition temperature of the XX0 model was obtained as $T_{\rm BKT} = 0.699J/k_{\rm B}$ [50], which is lower than the usual (two-component) XY model $T_{\rm BKT} = 0.898J/k_{\rm B}$ [59]. This is naturally understood due to the difference of the degree of freedom of these models.

Our numerical result is shown in Fig. 4. The size dependance of C is actually small. We estimate the BKT transition temperature $T_{\rm BKT}$ by two methods, one by using the data of χ and the other by using Υ. We plot $\chi/L^{7/4}$ for some values of L as a function of βt by assuming $\eta = 1/4$, in which the crossing point of the curves gives $T_{\rm BKT}$. From Υ, we take the temperatures that correspond to the crossing points of $\Upsilon(T)$ and the line $\Upsilon = (2/\pi)k_{\rm B}T_{\rm BKT}$ related to the universal jump value for various values of L, interpolating them to $L \to \infty$. Both these methods give the same $T \approx 0.702J/k_{\rm B}$, which is consistent with the result of Ref. [50] and confirms the accuracy of our numerical computations.

2. f=1/2

We next consider the case with full frustration $f = 1/2$. If there is a continuous phase transition, various quantities should exhibit a singular behavior near the transition temperature T_c. Figure 5(a) represents the specific heat C as a function of βt, where C exhibits a peak structure as a function of βt and the height of the peak increases with increasing L. This suggests the occurrence of a second-order phase transition. Concurrently, χ and Υ grow from zero with increasing βt, which is a signature of the emergence of superfluid order. Hence, the qualitative feature of the phase transition is similar to the FFXYM.

It is important to clarify whether the nature of the phase transition is consistent with those observed in the analysis of the FFXYM. In the FFXYM, two separate phase transitions may occur, corresponding to the breaking of the Z_2 chirality and the U(1) symmetry [31–41]. It is still inconclusive whether the former obeys the universality class of the Ising transition and the latter is subject to the BKT mechanism with non-universal jump of the helicity modulus.

First, we focus on the data of the specific heat to clarify the Z_2-related phase transition. To determine the critical temperature and the critical exponents, we use finite-size scaling analysis [60], where the specific heat C is expressed as

$$C(L, \tilde{t}) = L^{\alpha/\nu}\tilde{\phi}(L^{1/\nu}\tilde{t}), \tag{43}$$

where $\tilde{t} = (T - T_c)/T_c$ is a reduced temperature, α the standard exponent for the specific heat, and ν the exponent for the divergence of the correlation length. Since the scaling functions $\tilde{\phi}$ should depend on a single variable, we can make all the data for each system size L fall on the same curve by appropriately adjusting the values of the critical exponents α, ν and T_c. For a finite lattice

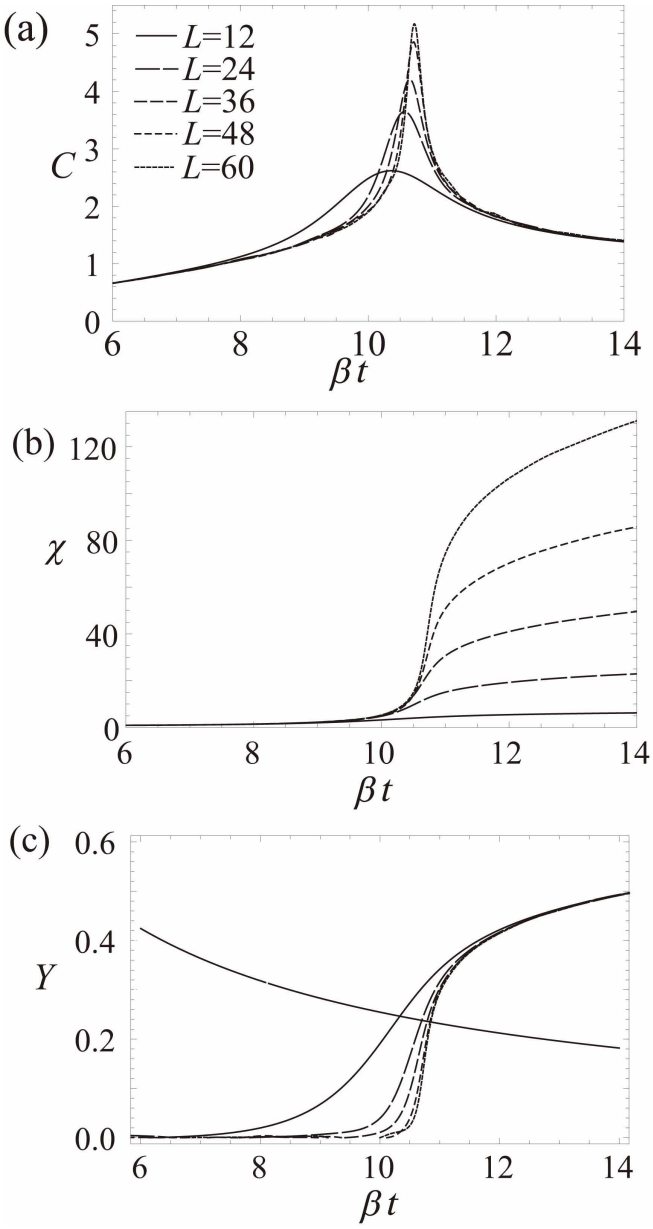

FIG. 5: Several thermodynamic quantities for f=1/2: (a) The specific heat C, (b) the in-plane susceptibility χ, and (c) the helicity modulus Υ for the CP^1 model with $\mu = 0$ and $f = 1/2$ as a function of βt. The system size for each curve is $L = 12$, 24, 36, 48, 60. An additional curve $\Upsilon = 8/\pi\beta t$ in (c) indicates the universal jump of a BKT transition.

the peak in the specific heat scales with system size as $C_{\rm max} \propto L^{\alpha/\nu}$ and occurs at the temperature where the scaling function $\tilde{\phi}(L^{1/\nu}\tilde{t})$ is maximum, defining the finite-lattice transition temperature $T_c(L) = T_c + {\rm const} \times L^{-1/\nu}$.

The obtained scaling functions are plotted in Fig. 6 for both the FFXYM and the gauged CP^1 model. For the FFXYM, we obtain $T_c = 0.454J/k_{\rm B}$, $\nu = 0.873$ and $\alpha = 0.383$ from Fig. 6(a), which is consistent with the hyperscaling relation $d\nu = 2 - \alpha$ (d is the dimension

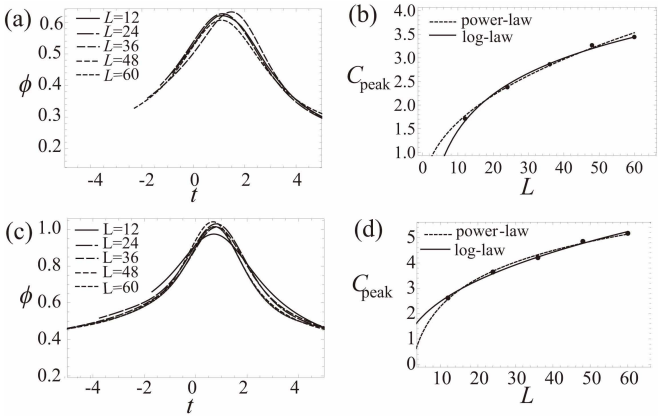

FIG. 6: The left panels show the power-law scaling collapse of the specific heat data for (a) FFXYM and (c) gauged CP^1 model. The right panels show the power-law and logarithmic fitting of the specific heat peak with respect to sizes L for (b) FFXYM and (d) the gauged CP^1 model. The power-law fitted value is $\alpha/\nu = 0.439$ for (a) and $\alpha/\nu = 0.397$ for (c).

.

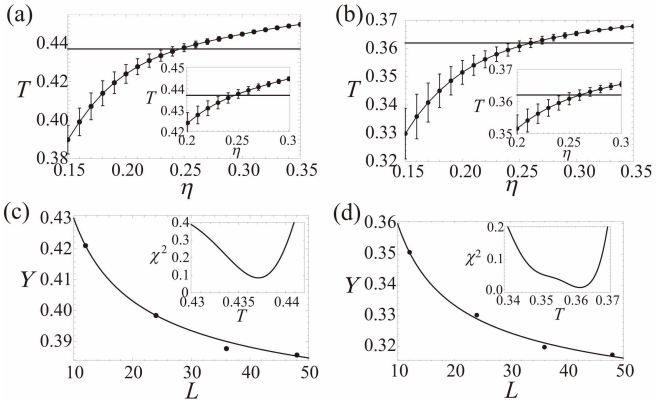

FIG. 7: Data of the BKT transition of the FFXYM [(a) and (c)] and the gauged CP^1 model for $f = 1/2$ [(b) and (d)]. In (a) and (b), we show $T_{\rm BKT}$ obtained by method (i) (see the text) by the horizontal line; (a) $T = 0.437J/k_{\rm B}$ and (b) $T = 0.363J/k_{\rm B}$. In addition, the temperature corresponding to the crossing point in the method (ii) is plotted as a function of η. Figures (c) and (d) show the best fit of the scaling relation Eq. (39) at the corresponding $T_{\rm BKT}$, which is obtained by finding the minimum of χ^2-fit error shown in the inset.

.

number). Our scaling analyses support the non-Ising exponent $\nu < 1$, which is consistent with some of the literature [32–34, 36]. However, it should be noted that there have been several claims that this non-Ising exponent is caused by the artifact of the finite-size effect and the exponent in the infinite system may be the Ising one $\nu = 1$ [35, 39, 41]. Since our calculation does not have enough system size to resolve this problem and we cannot distinguish the data of Fig. 6(a) as a power-law fitting or logarithmic fitting [see Fig. 6(b)], we shall not go to discuss the details of this issue. Our main claim in this work is that the similar behavior also occurs for the gauged CP^1 model. For this model, we also extract the critical exponents from the same analysis for Fig. 6 (c) and (d) as $T_c = 0.369J/k_{\rm B}$, $\nu = 0.878$ and $\alpha = 0.349$. The transition temperature becomes lower than that for the FFXYM, while the critical exponents are similar.

Next, we study the U(1)-related phase transition by employing the same analysis for the $f = 0$ case. Some studies revealed that the jump size of Υ at $T = T_{\rm BKT}$ may be non-universal for the FFXYM [31–34, 41]. Here, we do not assume $\eta = 1/4$ and evaluate $T_{\rm BKT}$ with two different methods: (i) Using the χ^2-fit of the scaling relation Eq. (39), we evaluate $T_{\rm BKT}$ and the jump size $T^*_{\rm BKT}$ at $T_{\rm BKT}$, which gives the exponent $\eta = T_{\rm BKT}/4T^*_{\rm BKT}$. (ii) We plot $\chi/L^{2-\eta}$ as a function of βt for several system sizes L and take the temperature at the crossing point. We make this analysis by varying η around 1/4 and search the value of η that gives the same $T_{\rm BKT}$ obtained in the analysis (i). The summary of this analysis is shown in Fig. 7. For the FFXYM, the scaling analysis (i) alone gives $T_{\rm BKT} = 0.437J/k_{\rm B}$ and $\eta = 0.2$. This is consistent with the previous literature, where $T_{\rm BKT} = 0.437J/k_{\rm B}$ is slightly lower than T_c and the BKT jump is non-universal [31–34, 41]. However, the crossing point obtained by the analysis (ii) is preferable to $\eta \approx 0.25$, as shown in Fig. 7(a), which suggests the same universality of the conventional BKT transition. This usual BKT behavior for the FFXYM was also suggested by Olsson [35]. Similar behavior is also found for the gauged CP^1 model as $T_{\rm BKT} = 0.363J/k_{\rm B}$ and $\eta \approx 0.22$ for the analysis (i) and $\eta \approx 0.26$ for the analysis (ii).

3. f=2/5

The thermodynamic properties for $f = 2/5$ would appear to be similar to the $f = 1/2$ situation as seen in Fig. 8. However, the nature of the phase transition is very different. In the FXYM, several works indicated that the transition is associated with first-order type [43, 45]. Li and Teitel observed hysteresis of the internal energy when the temperature was cycled around the transition and used this as an argument for a first-order transition [43]. Denniston and Tang pointed out that the complicated branching structure of domain walls is similar to the $q > 5$ Pott's models where the first-order transition occurs [45]. The most direct indication of a first-order transition is the presence of a free energy barrier between the ordered and disordered states which diverges as the system size increases [45]. Since there is no diverging characteristic length to which the linear dimension L could be compared at a first-order transition, one finds that it is simply the volume L^2 that controls the size effects.

In the gauged CP^1 model, Fig. 8(a) clearly shows the rapid growth of the peak of C. The inset of Fig. 8(b) shows the peak values of C as a function of L^2. The linear

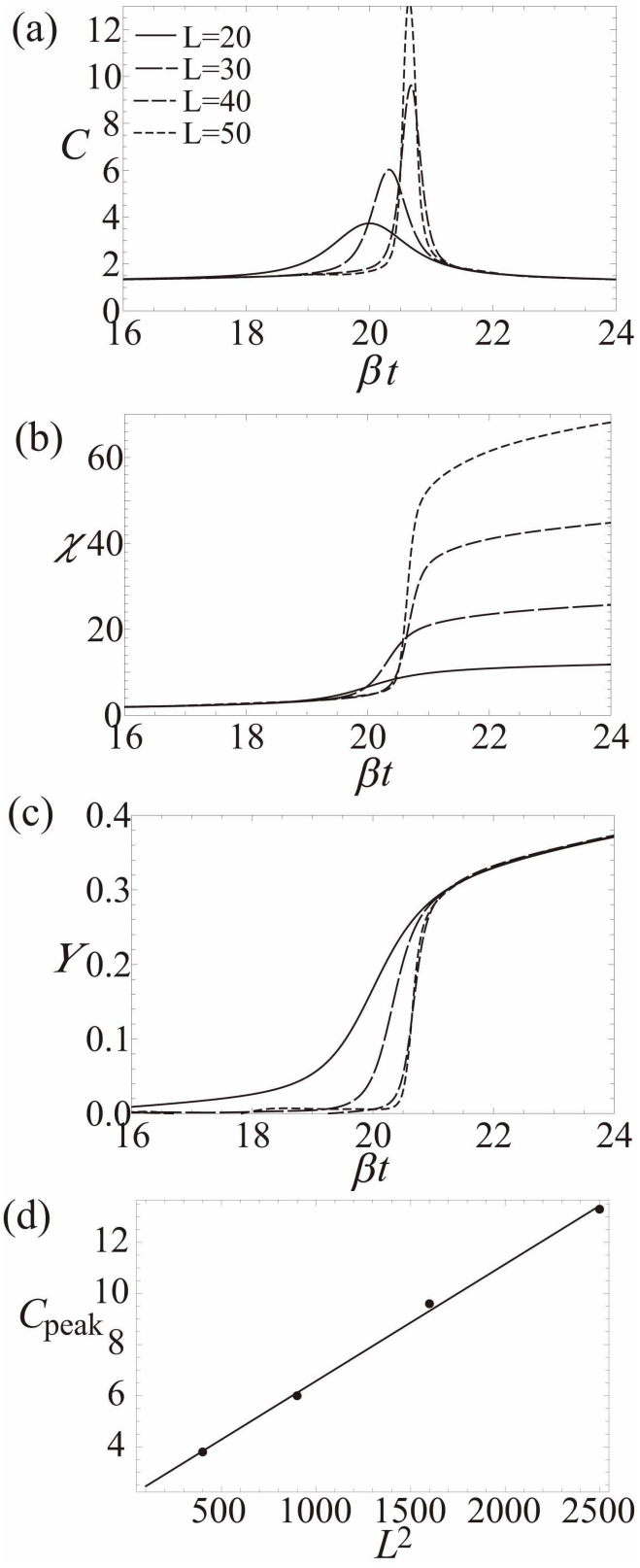

FIG. 8: Several thermodynamic quantities for the CP^1 model with $\mu = 0$ and $f = 2/5$ as a function of βt. (a) The specific heat C, (b) the in-plane susceptibility, and (c) the helicity modulus Υ. The system size for each curve is $L = 20$, 30, 40, 50. (d) represents specific heat vs L^2

.

fit clearly shows the expected first-order scaling behavior. From the positions of the peaks as a function of L, we obtain $T_c = 0.193J/k_{\rm B}$, which is again slightly lower than that of the FXYM $T_c = 0.2127J/k_{\rm B}$ [45]. The growing χ and Υ at low temperature certainly provides the emergence of the superfluid order. Due to the presence of the first-order transition, it is difficult to explicitly discuss the properties of the BKT transition.

C. The case of non half-filling ($\mu \neq 0$)

Finally, we show the similar data with the previous subsection but for $\mu \neq 0$, where the particle occupation at each site is not half-filling. In terms of the pseudospin Hamiltonian (10), this situation corresponds to applying a longitudinal magnetic field, as seen in the second term of Eq. (10).

We make the similar analysis as in the previous calculation for $\mu = 0.7$, where the averaged density is about $\rho \approx 0.7$-0.8, which depends weakly on f and βt. The thermodynamic quantities behave similarly to those found in the half-filling case; an example for $\mu = 0.7$ and $f = 1/2$ is shown in Fig. 9. We find no qualitative difference in the phase transition for each f from the $\mu = 0$ case. We show in Table I the obtained critical exponents ν, α and $\eta(T_{\rm BKT})$ and the critical temperatures T_c and $T_{\rm BKT}$ associated with the Z_2 and U(1) symmetry breaking, respectively. One can see that the transition temperature is further reduced from the $\mu = 0$ case. Also, the critical exponents are modified from the values of $\mu = 0$. This is naturally understood as follows. As one increases $|\mu|$, the average magnitude of the XY spin component $[(s_i^x)^2 + (s_i^y)^2]^{1/2}$ decreases because $|s_i^z|$ increases (For example, the limit $\mu \to \pm\infty$ implies $s_z = \pm 1$). If the length of XY spin is fixed, the model should be in the same universality class as the FXYM. However, our study for $\mu = 0$ and $f = 1/2$ exhibits that the fluctuations of $s_i^{x,y}$ give rise to critical exponents different from those of the FFXYM. Therefore fluctuations around the XY spins of different length may certainly produce different critical exponents.

V. CONCLUSION AND DISCUSSION

We study the finite-temperature phase structures of hard-core bosons in a two-dimensional optical lattice subject to an effective magnetic field by employing the gauged CP^1 model. Based on the multicanonical Monte Carlo simulations, we study their phase structures at finite temperatures for several values of the magnetic flux per plaquette of the lattice and mean particle density. A summary of this work is listed in Table I. Also, the magnitudes of the particle density fluctuations are measured to be less than 20%. They cause the shift of transition temperatures T_c and $T_{\rm BKT}$, which are slightly decreased from those of the FXYM, and also the shift of critical

TABLE I: List of the transition temperatures and some critical exponents obtained in this work. The transition temperature is measured by using $J = t\rho(1-\rho)$; for $\mu \neq 0$, ρ is used at the corresponding transition temperature. In $\eta(T_{\rm BKT})$, we represent two values obtained by the method (i) and (ii) in Sec. IV B 2. For comparison, the corresponding values for the 2D Ising model are $\nu = 1$ and $\alpha = 0$, which implies the logarithmic divergence of the specific heat.

	$T_{\rm c}$	ν	α	$T_{\rm BKT}$	$\eta(T_{\rm BKT})$
CP^1 model, $f = 0$, $\mu = 0$	—	—	—	0.702(1) $J/k_{\rm B}$	0.25
CP^1 model, $f = 1/2$, $\mu = 0$	0.369(4) $J/k_{\rm B}$	0.878(5)	0.349(9)	0.363(3) $J/k_{\rm B}$	(i) 0.22, (ii) 0.26
CP^1 model, $f = 2/5$, $\mu = 0$	0.193(1) $J/k_{\rm B}$	—	—	—	—
CP^1 model, $f = 0$, $\mu = 0.7$	—	—	—	0.672(1) $J/k_{\rm B}$	0.25
CP^1 model, $f = 1/2$, $\mu = 0.7$	0.347(1) $J/k_{\rm B}$	0.781(25)	0.381(7)	0.334(4)$J/k_{\rm B}$	(i) 0.19, (ii) 0.24
CP^1 model, $f = 2/5$, $\mu = 0.7$	0.168(1) $J/k_{\rm B}$	—	—	—	—
2D XY model	—	—	—	0.898(1) $J/k_{\rm B}$	0.25
2D FFXYM	0.454(1) $J/k_{\rm B}$	0.873(3)	0.383(34)	0.437(3) $J/k_{\rm B}$	(i) 0.2, (ii) 0.25

exponents α and ν. However these fluctuations do not modify the global phase structure and the critical properties of FXYM.

The regime described by the XY model (Josephson junction array) can be realized when the mean particle number at each site is very large $\rho_i \gg 1$ [28, 61], where the particle number fluctuation becomes negligible as $\sim \rho_i^{-1/2}$. The BKT transition in such a regime was observed by Schweikhard et al. [62]. The important message of this work is that, even though the strong particle number fluctuation becomes remarkable due to the small site occupation $\rho_i \sim 1$, one can expect similar thermal phase transitions seen in the FXYM. The recent experimental demonstration on generating an effective magnetic field in an optical lattice [8] opens the door to explore the rich finite-temperature phase diagram of this system.

Acknowledgments

The authors thank Shu Tanaka for useful discussions. One of the authors (K.K.) is supported in part by a Grant-in-Aid for Scientific Research (Grant No. 21740267) from MEXT, Japan.

Appendix A: Symmetry of the gauged CP^1 model

We summarize the symmetry properties of the gauged CP^1 model Eq. (24), from which one can get some useful information to understand the results.

The model equation (24) or (25) has the following symmetry properties:

1. The model has global U(1) symmetry; it is invariant under the change $\phi_i \to \phi_i' = e^{i\theta}\phi_i$.

2. The model also has local gauge symmetry. If we change the gauge $\mathbf{A} \to \mathbf{A} + \nabla\chi$, then the Hamiltonian remains unchanged if the boson picks up a phase change as $A_{ij} \to A_{ij} + (\chi_j - \chi_i)$ and $\phi_i \to e^{i\chi_i}\phi_i$. In terms of the pseudospin $\vec{s}_i$ for the i-th site, this corresponds to a rotation with the angle χ_i in the xy plane, $s_i^{\pm} \to e^{\mp i\chi_i} s_i^{\pm}$. Because the choice $\chi_i = \pi i_x i_y$ gives rise to a shift of fluxes $f \to f + 1$, the system is periodic in f with the period 1.

3. The Hamiltonian Eq. (24) is invariant under the change $f \to f' = -f$, corresponding to the time reversal operation $\phi_i \to \phi' = \phi_i^*$ ($\lambda_{ai} \to \lambda'_{ai} = -\lambda_{ai}$). Since the partition function is not affected by this transformation, one can show that the internal energy $E = \langle H\rangle = -\partial \ln Z/\partial\beta$ and the mean number density $\rho = \langle N\rangle/L^2 = L^{-2}\partial \ln Z/\partial(\beta\mu)$ have the following properties

$$E(\beta, t, \mu, f) = E(\beta, t, \mu, -f), \tag{A1}$$
$$\rho(\beta, t, \mu, f) = \rho(\beta, t, \mu, -f). \tag{A2}$$

The symmetric form of the ground state energy shown in Fig. 1 can be understood as follows. The plotted energy $E_{\rm min}$ in Fig. 1 is the first term of Eq. (24) $E = E_{\rm min} - \mu\rho L^2$. From Eq. (A2), one can see $\mu(\rho(f), \beta, t, f) = \mu(\rho(-f), \beta, t, -f)$. For the fixed ρ, Eq. (A1) gives

$$\begin{aligned} E_{\rm min}(t, \mu(f), f) &= E_{\rm min}(t, \mu(-f), -f) \\ &= E_{\rm min}(t, \mu(1-f), 1-f). \end{aligned} \tag{A3}$$

The last equality is due to the invariance for $f \to f + 1$.

4. Let us consider the transformation $\psi_i \to \psi_i' = \pi - \psi_i$. Then, Eq. (28) yields $H_{CP^1}(\mu) \to H'_{CP^1}(\mu) = H_{CP^1}(-\mu)$ and $\rho = \langle\cos^2(\psi/2)\rangle \to \rho'(\mu) = 1 - \rho(-\mu)$ (or equivalently $s_i^z \to s_i'^z = -s_i^z$). This reflects the particle-hole symmetry, where ρ' should be interpreted as the hole density if ρ represents the particle density. Therefore, especially for $\mu = 0$, we obtain the relation

$$\rho(\beta, t, 0, f) = \rho'(\beta, t, 0, f) = 1 - \rho(\beta, t, 0, f) = \frac{1}{2}. \tag{A4}$$

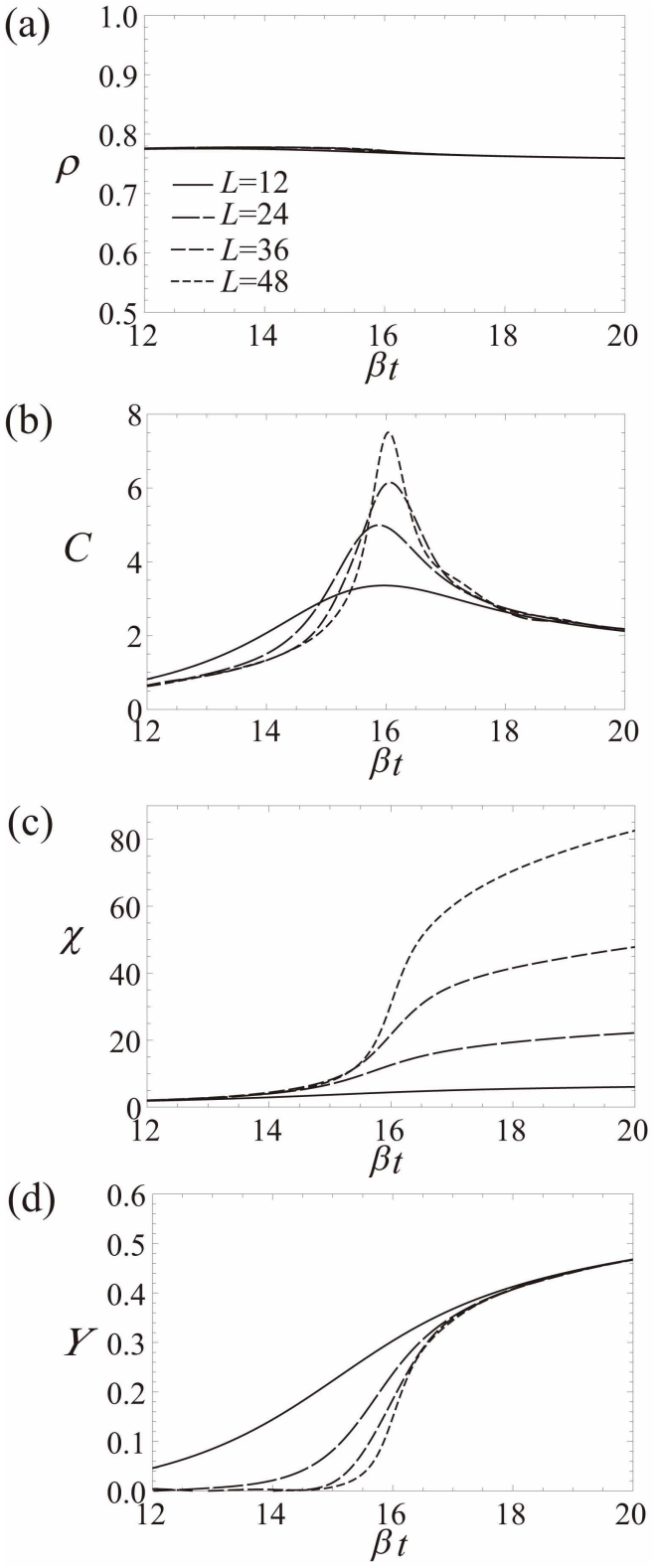

FIG. 9: Several thermodynamic quantities for the CP^1 model with $\mu = 0.7$ and $f = 1/2$ as a function of βt. (a) mean particle number ρ (b) The specific heat C, (c) the in-plane susceptibility χ, and (d) the helicity modulus Υ. The system size for each curve is $L = 12$, 24, 36, 48.

.

[1] I. Bloch, J. Dalibard, and W. Zwerger, Rev. Mod. Phys. **80**, 885 (2008).
[2] N. R. Cooper, Adv. Phys. **57**, 539 (2008).
[3] S. Tung, V. Schweikhard, and E.A. Cornell, Phys. Rev. Lett. **97**, 240402 (2006).
[4] R. A. Williams, S. Al-Assam, C. J. Foot, Phys. Rev. Lett. **104**, 050404 (2010).
[5] J. Dalibard, F. Gerbier, G. Juzeliūnas, and P. Öhberg, arXiv:1008.5378 (2010).
[6] Y.-J. Lin, R. L. Compton, A. R. Perry, W. D. Phillips, J. V. Porto, and I. B. Spielman Phys. Rev. Lett. **102**, 130401 (2009).
[7] Y. Lin, R. L. Compton, K. J. Garcia, J. V. Porto, and I. B. Spielman, Nature(London), **462**, 628 (2009).
[8] M. Aidelsburger, M. Atala, S. Nascimbène, S. Trotzky, Y.-A. Chen, I. Bloch, Phys. Rev. Lett. **107**, 255301 (2011).
[9] D. Jaksch and P. Zoller, New J. Phys. **5**, 56 (2003).
[10] E. J. Mueller, Phys. Rev. A **70**, 041603(R) (2004).
[11] A. S. Sørensen, E. Demler, and M. D. Lukin, Phys. Rev. Lett. **94**, 086803 (2005).
[12] F. Gerbier and J. Dalibard, New J. Phys. **12**, 033007 (2010).
[13] M. Ö. Oktel, M. Nita, and B. Tanatar Phys. Rev. B **75**, 045133 (2007).
[14] R. O. Umucalilar and M. Ö. Oktel Phys. Rev. A **76**, 055601 (2007).
[15] D. S. Goldbaum and E. J. Mueller, Phys. Rev. A **77**, 033629 (2008); *ibid* **79**, 021602 (2009).
[16] R. N. Palmer, A. Klein, and D. Jaksch, Phys. Rev. A **78**, 013609 (2008).
[17] T. P. Polak and T. K. Kopeć Phys. Rev. A **79**, 063629 (2009).
[18] G. Möller and N. R. Cooper, Phys. Rev. Lett. **103**, 105303 (2009).
[19] R. O. Umucalilar and E. J. Mueller Phys. Rev. A **81**, 053628 (2010) .
[20] T. Durić and D. K. K. Lee, Phys. Rev. B **81**, 014520 (2010).
[21] S. Powell, R. Barnett, R. Sensarma, and S. Das Sarma Phys. Rev. Lett. **104**, 255303 (2010), Phys. Rev. A **83**, 013612 (2011).
[22] G. Möller and N. R. Cooper, Phys. Rev. A **82**, 063625 (2010).
[23] J. Zhang, C.-M. Jian, F. Ye, and H. Zhai, Phys. Rev. Lett. **105**, 155302 (2010).
[24] D. R. Hofstadter, Phys. Rev. B **102**, 070403 (2010).
[25] E. Brown, Phys. Rev. **133**, A1038 (1964).
[26] J. Zak, Phys. Rev. **134**, A1602 (1964); *ibid.* **134**, A1607 (1964).
[27] M. Polini, R. Fazio, A. H. MacDonald, and M. P. Tosi, Phys. Rev. Lett. **95**, 010401 (2005).
[28] K. Kasamatsu, Phys. Rev. A. **79**, 021604(R) (2009).
[29] C. Chin, R. Grimm, P. Julienne, and E. Tiesinga, Rev. Mod. Phys. **82**, 1225 (2010).
[30] Y. Nakano, T. Ishima, N. Kobayashi, K. Sakakibara, I. Ichinose, and T. Matsui, Phys. Rev. B **83**, 235116 (2011).
[31] S. Teitel and C. Jayaprakash, Phys. Rev. B **27**, 598 (1983).
[32] J. Lee, J. M. Kosterlitz and E. Granato, Phys. Rev. B **43**, 11531 (1991).
[33] G. Ramirez-Santiago and J. V. José, Phys. Rev. B **49**, 9567 (1994).
[34] S. Lee and K.-C. Lee, Phys. Rev. B **49**, 15184 (1994).
[35] P. Olsson, Phys. Rev. Lett. **75**, 2758 (1995).
[36] H.J. Luo, L. Schülke, and B. Zheng, Phys. Rev. Lett. **81**, 180 (1998)
[37] S. E. Korshunov, Phys. Rev. Lett. **88**, 167007 (2002).
[38] M. Hasenbusch, A. Pelissetto, and E. Vicari, Phys. Rev. B **72**, 184502 (2005).
[39] P. Olsson and S. Teitel, Phys. Rev. B **71**, 104423 (2005).
[40] P. Minnhagen, B.J. Kim, S. Bernhardsson, and G. Cristofano, Phys. Rev. B **78**, 184432 (2008).
[41] S. Okumura, H. Yoshino, and H. Kawamura, Phys. Rev. B **83**, 094429 (2011).
[42] G. S. Grest, Phys. Rev. B **39**, 9267 (1989).
[43] Y.-H. Li and S. Teitel, Phys. Rev. Lett. **65**, 2595 (1990).
[44] S. Lee and K.-C. Lee, Phys. Rev. B **52**, 6706 (1995).
[45] C. Denniston and C. Tang, Phys. Rev. B **58**, 6591 (1998).
[46] A. Shimizu, K. Aoki, K. Sakakibara, I. Ichinose, and T. Matsui, Phys. Rev. B **83**, 064502 (2011).
[47] We use the term "gauged" to describe the constant gauge field A_{ij} in the present model. This usage should be distinguished from the related "gauge models" [30, 46] in which a dynamical U(1) gauge field is involved.
[48] We note that definition of the O(3) spin vector $\vec{s}_i$ has no factor 1/2 of the SU(2) operator $\hat{s}_i^{x,y,z}$ of Eq. (19) to ensure $\vec{s}_i\vec{s}_i = 1$. Even if we consider $(1/2)\vec{s}_i$, its squared magnitude $(1/4)\vec{s}_i\vec{s}_i$=1/4 is different from 3/4 in Eq. (19) reflecting the quantum fluctuations in the expression $s(s+1) = s^2 + s$.
[49] N. H. Lindner, A. Auerbach, and D. P. Arovas, Phys. Rev. Lett. **102**, 070403 (2009), Phys. Rev. B, **82**, 134510 (2010).
[50] A. Cuccoli, V. Tognetti, and R. Vaia, Phys. Rev. B **52**, 10221 (1995).
[51] T. Kawasaki and S. Miyashita, Prog. Theor. Phys. **93**, 47 (1995).
[52] S. Teitel and C. Jayaprakash, Phys. Rev. Lett. **51**, 1999 (1983).
[53] T. C. Halsey, Phys. Rev. B **31**, 5728 (1985).
[54] J. P. Straley and G. M. Barnett, Phys. Rev. B **48**, 3309 (1993).
[55] B. A. Berg, Fields Inst. Commun. **26**, 1 (2000).
[56] D. R. Nelson and J. M. Kosterlitz, Phys. Rev. Lett. **39**, 1201 (1977).
[57] H. Weber and P. Minnhagen, Phys. Rev. B **37**, 5986 (1988).
[58] P. Minnhagen, Phys. Rev. Lett. **54**, 2351 (1985).
[59] R. Gupta, J. DeLapp, G. G. Batrouni, G. C. Fox, C. F. Baillie, and J. Apostolakis, Phys. Rev. Lett. **61**, 1996 (1988).
[60] See, e.g., *Finite Size Scaling and Numerical Simulation of Statistical Systems*, ed. V. Privman (World Scientific, Singapore, 1990), and references cited therein.
[61] A. Trombettoni, A. Smerzi, and P. Sodano, New J. Phys. **7**, 57 (2005).
[62] V. Schweikhard, S. Tung, and E. A. Cornell, Phys. Rev. Lett. **99**, 030401 (2007).